A SAMPLING STRATEGY FOR RECENT AND FOSSIL BRACHIOPODS: SELECTING THE OPTIMAL SHELL SEGMENT FOR GEOCHEMICAL ANALYSES

MARCO ROMANIN[1*], GAIA CRIPPA[2], FACHENG YE[2], UWE BRAND[3], MARIA ALEKSANDRA BITNER[1], DANIÈLE GASPARD[4], VERENA HÄUSSERMANN[5] & JÜRGEN LAUDIEN[6]

[1*]Corresponding author. Institute of Paleobiology, Polish Academy of Sciences, Twarda 51/55, 00-818 Warsaw, Poland. E-mail: m.romanin@twarda.pan.pl; bitner@twarda.pan.pl
[2]Università degli Studi di Milano, Dipartimento di Scienze della Terra 'A. Desio', via Mangiagalli 34, Milano, 20133, Italy. E-mail: gaia.crippa@unimi.it; facheng.ye@unimi.it
[3]Department of Earth Sciences, Brock University, 1812 Sir Isaac Brock Way, St. Catharines, ON Canada L2S 3A1. E-mail: ubrand@brocku.ca
[4]Museum National d'Histoire Naturelle, Département Origines et Evolution, UMR CNRS-MNHN-UPMC 7207, Centre de Recherche sur la Paléodiversité et les Paléoenvironnements (CR2P), 8 Rue Buffon, 75231 Paris Cedex 05, France.E-mail: daniele.gaspard@mnhn.fr
[5]Pontificia Universidad Católica de Valparaíso, Facultad de Recursos Naturales, Escuela de Ciencias del Mar, Avda. Brasil 2950, Valparaíso, Chile and Huinay Scientific Field Station. E-mail: v.haussermann@gmail.com
[6]Alfred-Wegener-Institut Helmholtz-Zentrum für Polar- und Meeresforschung, Bremerhaven, Germany. E-mail: juergen.laudien@awi.de

Abstract. Recent and fossil brachiopod shells have a long record as biomineral archives for (palaeo)climatic and (palaeo)environmental reconstructions, as they lack or exhibit limited vital effects in their calcite shell and generally are quite resistant to diagenetic alteration. Despite this, only few studies address the issue of identifying the best or optimal part of the shell for geochemical analyses. We investigated the link between ontogeny and geochemical signatures recorded in different parts of the shell. To reach this aim, we analysed the elemental (Ca, Mg, Sr, Na) and stable isotope ($\delta^{18}O$, $\delta^{13}C$) compositions of five recent brachiopod species (*Magellania venosa, Liothyrella uva, Aerothyris kerguelensis, Liothyrella neozelanica* and *Gryphus vitreus*), spanning broad geographical and environmental ranges (Chile, Antarctica, Indian Ocean, New Zealand and Italy) and having different shell layer successions (two-layer and three-layer shells). We observed similar patterns in the ventral and dorsal valves of these two groups, but different ontogenetic trends by the two- and three-layer shells in their trace element and stable isotope records. Our investigation led us to conclude that the optimal region to sample for geochemical and isotope analyses is the middle part of the mid-section of the shell, avoiding the primary layer, posterior and anterior parts as well as the outermost part of the secondary layer in recent brachiopods. Also, the outermost and innermost rims of shells should be avoided due to diagenetic impacts on fossil brachiopods.

INTRODUCTION

Brachiopods have a proven record with their shells storing important geochemical signatures of stable isotopes (oxygen and carbon) and trace elements (TE) (e.g., Carpenter & Lohmann 1995; Brand et al. 2003, 2011), rare earth elements (REE) (e.g., Azmy et al. 2011; Zaki et al. 2015), and of course other tracers (i.e. strontium, clumped, magnesium isotopes). They precipitate their generally low-magnesium calcite (LMC) shells in brachiopod isotopic equilibrium with ambient seawater exerting no or a limited vital effect, although different be-

haviours are observed in different shell layers/segments (e.g., Carpenter & Lohmann 1995; Auclair et al. 2003; Parkinson et al. 2005; Cusack et al. 2012; Brand et al. 2013, 2015; Bajnai et al. 2018). They are not abundant in modern seas and oceans, where they are mainly represented by the Order Terebratulida (Curry & Brunton 2007; Emig et al. 2013). In contrast, they dominated the benthic communities during the Palaeozoic, where many orders were present (Williams et al. 1997). For this reason, in recent years, there has been growing interest and use of fossil and recent brachiopod shells as high resolution biomineral archives for environmental and (palaeo)climatic reconstructions in the recent and distant past (e.g., Popp et al. 1986; Grossman et
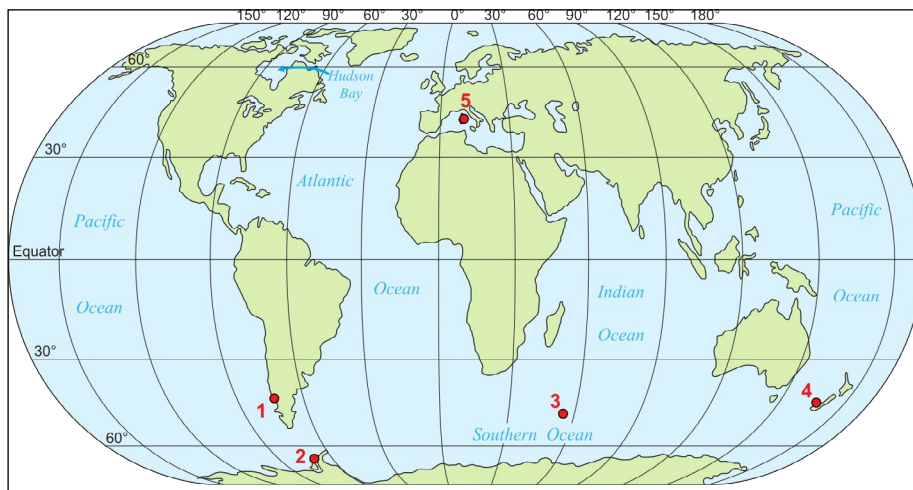
Fig. 1 - Map showing the localities of the specimens analysed in this study: 1) *Magellania venosa*, Comau fjord, Chile (South Pacific), 2) *Liothyrella uva*, off Rothera Island, Antarctica (Southern Ocean), 3) *Aerothyris kerguelensis*, off South Cochons Island (Indian Ocean), 4) *Liothyrella neozelanica*, off New Zealand coast (South Pacific); 5) *Gryphus vitreus*, off Montecristo Island, Italy (Mediterranean Sea).

al. 1991; Veizer et al. 1999; Brand 2004; Parkinson et al. 2005; Came et al. 2007; Angiolini et al. 2008, 2009; Brand et al. 2011; Cusack & Pérez-Huerta 2012; Garbelli et al. 2017; Ye et al. 2018), as well as tracers of diagenetic processes (Brand & Veizer 1980, 1981; Casella et al. 2018).

Terebratulid brachiopods form two- or three-layer mineralised shells, consisting of primary and secondary layers, or of primary, secondary and tertiary layers (e.g., Gaspard 1986; Gaspard & Nouet 2016; and see Fig. 1 in Ye et al. 2018). Although LMC of brachiopod shells seems ideal for geochemical analyses as it is generally resistant to diagenetic alteration (Lowenstam 1961; Popp et al. 1986; Brand et al. 2011), our increased understanding suggests that the different microstructures, composed of primary, secondary and tertiary shell layers, are not spatially homogenous in respect to their trace element concentrations and stable isotope compositions (Cusack et al. 2008, 2012; Rollion-Bard et al. 2016). The microcrystalline calcite of the primary layer is not secreted in isotopic equilibrium with seawater during biogenic precipitation and furthermore its Mg content falls outside the limits defining LMC (~5% mol $MgCO_3$; Veizer 1992; Carpenter & Lohmann 1995). Buening & Carlson (1992) observed deviations from the 'norm' in the Mg contents of the umbonal area. Furthermore, Brand et al. (2003, 2013) observed deviations in Mg content in several species as well as in some areas close to the anterior; changes in growth kinetics are a possible explanation (work in progress). On the other hand, fibres of the innermost secondary layer and the columnar calcite of the tertiary layer are deposited in brachiopod isotopic equilibrium with seawater (Parkinson et al. 2005; Cusack et al. 2012; Brand et al. 2013, 2015) and are the most

suitable components for environmental reconstructions, if diagenetic alteration can be ruled out for fossil specimens (Ye et al. 2018). Regions within the shell, such as the umbonal and muscle scar areas, can also have an impact on geochemical results if not removed from the studied material, mainly resulting in negative shifts in their $\delta^{18}O$ and $\delta^{13}C$ values and extraneous Mg contents probably linked to growth-related kinetics (Buening & Carlson, 1992; Carpenter & Lohmann 1995; Brand et al. 2003; Parkinson et al. 2005; Bajnai et al. 2018).

The high complexity in brachiopod shell microstructure and chemistry requires standardised analytical sampling procedures to correctly interpret the multitude of information stored in this biomineral archive. Zaky et al. (2015) and Crippa et al. (2016a) addressed the issues of proper cleaning and preparation procedures to use for both recent and fossil brachiopod shells. However, only a few studies have investigated the link between shell ontogeny, microstructure and geochemistry to define the optimal part of the shell to sample for ontogenetic and (palaeo)environmental reconstructions (Pérez-Huerta et al. 2008; Butler et al. 2015; Takizawa et al. 2017; Ullmann et al. 2017; Ye et al. 2018).

The aim of this study is to identify the optimal part of the shell for geochemical analyses without incurring a major bias from biochemical and biological processes of the organism or from external forces (e.g., fish farms, tectonic upheaval). To achieve this purpose, we analysed trace elements (Mg, Sr and Na) and stable isotopes ($\delta^{18}O$, $\delta^{13}C$) intrashell compositions of five recent brachiopod species: *Aerothyris kerguelensis* (Davidson, 1878), *Magellania venosa* (Solander, 1786), *Liothyrella uva* (Broderip, 1833), *Liothyrella neozelanica* (Thomson, 1918) and *Gryphus*

Species	#-Layers	Length (mm)	Location	Coordinates	Depth (m)	SW-^{18}O (‰)	Temperature (°C)	Salinity (psu)
Magellania venosa	2	37	Chile	42°22'29"S, 2°25'41.58"W	~20	-1.21	8 to 14	32.0
M. venosa (supplement)	2	70						
Liothyrella uva	2	47	Antarctica	67°34'11"S, 68°07'88"W	~10	-0.87	-1 to 1	32.8
Aerothyris kerguelensis	2	39	S. Cochons	46°13'04"S, 50°12'08"E	200-400	+0.5	4 to 8	-
Liothyrella neozelanica	3	70	New Zealand	34.707°S, 178.57°E	~1150	+0.3	3 to 7	34.5
Gryphus vitreus	3	47	Montecristo	42°55.035'N, 10°05.600'E	~150	+1.24	12 to 17	39.0

Tab. 1 - Species, shell structure (# of layers and ventral valve length), locality and seawater information. Note: length measured on the ventral valves as well as along the 'curved' growth axis.

vitreus (Born, 1778). They cover a wide geographical range respectively from the Indian Ocean to Chile to Antarctica to New Zealand to Italy, and have different shell layer successions (Table 1). The main goal of this study is to devise an approach which can be used not only in recent specimens, but also in fossil ones, in order to make the geochemical composition of fossil brachiopod shells a more reliable tool for palaeoclimatic and palaeoenvironmental reconstructions.
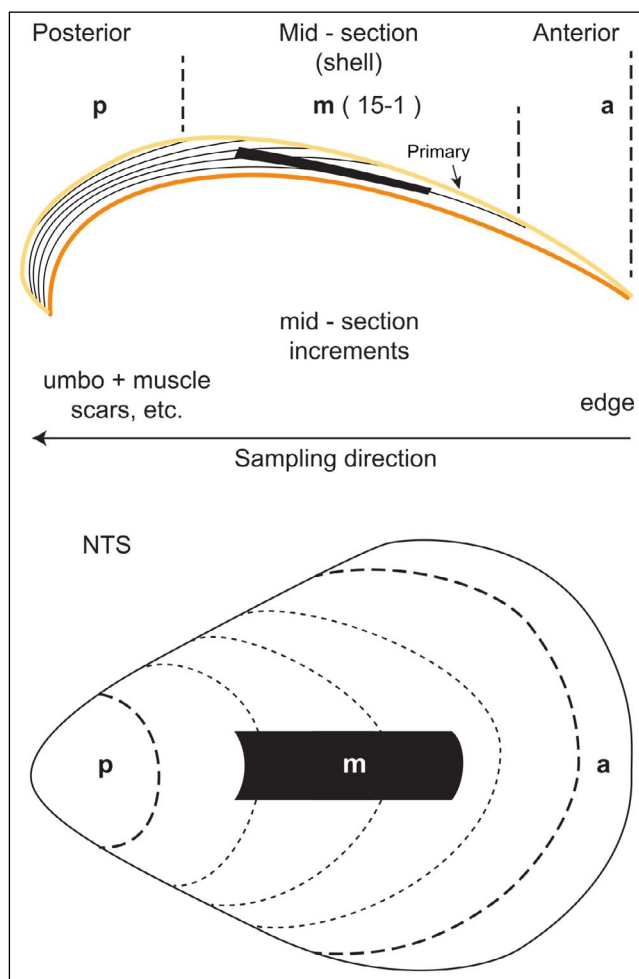

Fig. 2 - Schematic representation of cross section (upper image) and top view (lower image) of a brachiopod valve showing the posterior (p), middle (m) and anterior (a) parts of the shell. In yellow is highlighted the primary layer; in orange the innermost layers of the shell easily susceptible to alteration; the black area is intended to represent the suggested optimal sampling area. The direction of sampling is also illustrated on the profile. Note: M – mid-section sampling interval ranging from m1 adjacent to anterior (a) sample to m15 (or other) adjacent to the posterior (p, umbonal area) (see Appendix 1), Black line (side) and area (top) is the optimal sampling area, NTS – not to scale.

MATERIAL

Seven recent articulated brachiopod specimens belonging to five species of the Order Terebratulida were collected from five worldwide locations (Fig.1, Table 1, Appendix 1). All the species analysed have a punctate shell and may have a two- or three-layer shell successions. *Aerothyris kerguelensis* was sampled off south Cochons Island, Indian Ocean during the MD30 "BIOMASS" cruise, Station 29 (CP 82), at depths ranging from 200 to 400 m and an average water temperature of about 4.5°C (Table 1; Locarnini et al. 2013). *Magellania venosa* was collected at Comau fjord, Northern Patagonia, Chile from a depth of about 20 m and an average water temperature of about 11°C (Table 1). *Liothyrella uva* was collected off Rothera Island, Antarctica at an average depth of 10 m (Table 1). *Liothyrella neozelanica* was collected off New Zealand at a depth of about 1150 m (Table 1). *Gryphus vitreus* was collected off Montecristo Island, Italy from a water depth of about 150 m (Table 1). Specimen size ranged from 70 mm to 39 mm for the ventral valve with correspondingly smaller dorsal valves (Table 1). The three-layer shells were generally thicker than their two-layer counterparts and thus facilitating greater sampling interval.

METHODS

Sample preparation and sampling

All specimens were cleaned following the procedure of Zaky et al. (2015). Shells were washed with distilled water, then cleaned by immersion in hydrogen peroxide for up to three days. The remaining organic tissue and epibionts were physically removed and further cleaning of the exterior and interior surfaces and removal of the primary layer was achieved by leaching shells with 10 % hydrochloric acid (HCl) for about 5 seconds or until clean. Finally all shells were rinsed with deionized water and air dried. Sampling was performed along the growth axis

Species	Parameter	N	Mean	STD	Min	Max	p
Magellania venosa	Mg (V)	9	910	145	750	1176	0.564
	Mg (D)	8	945	89	825	1048	
	Sr (V)	9	1115	180	933	1490	0.742
	Sr (D)	8	1085	189	939	1511	
	$\delta^{13}C$ (V)	9	-0.66	2.06	-4.93	0.94	0.661
	$\delta^{13}C$ (D)	8	-0.26	1.60	-3.29	0.96	
	$\delta^{18}O$ (V)	9	-0.71	1.25	-3.15	0.19	0.574
	$\delta^{18}O$ (D)	8	-0.40	0.96	-2.10	0.40	
Aerothyris kerguelensis	Mg (V)	18	1177	394	694	2065	0.986
	Mg (D)	18	1175	324	787	2131	
	Sr (V)	18	875	116	696	1072	0.873
	Sr (D)	18	881	97	753	1093	
	Na (V)	18	1871	497	1220	2628	0.594
	Na (D)	18	1789	417	1220	2651	
	$\delta^{13}C$ (V)	10	2.48	0.21	2.00	2.68	0.421
	$\delta^{13}C$ (D)	10	2.56	0.22	2.13	2.78	
	$\delta^{18}O$ (V)	10	2.80	0.14	2.56	3.06	0.076
	$\delta^{18}O$ (D)	10	2.95	0.19	2.70	3.22	
Liothyrella uva	Mg (V)	12	2920	483.6	2202	4125	< **0.001**
	Mg (D)	12	1999	260.5	1784	2649	
	Sr (V)	12	1314	193.6	1056	1652	0.037
	Sr (D)	12	1177	73.1	1075	1282	
	Na (V)	12	2784	269.9	2445	3368	0.745
	Na (D)	12	2741	371.1	1770	3188	
	$\delta^{13}C$ (V)	12	0.99	0.26	0.32	1.27	0.832
	$\delta^{13}C$ (D)	12	1.02	0.26	0.33	1.31	
	$\delta^{18}O$ (V)	12	3.47	0.11	3.23	3.63	0.538
	$\delta^{18}O$ (D)	12	3.45	0.11	3.29	3.65	
Liothyrella neozelanica	Mg (V)	17	1425	395	1035	2644	0.592
	Mg (D)	13	1503	392	1121	2627	
	Sr (V)	17	670	89	571	921	0.381
	Sr (D)	13	701	103	582	972	
	Na (V)	16	1089	277	777	1743	0.701
	Na (D)	12	1133	326	816	1921	
	$\delta^{13}C$ (V)	17	2.31	0.46	1.57	2.82	0.729
	$\delta^{13}C$ (D)	13	2.25	0.55	1.39	2.89	
	$\delta^{18}O$ (V)	17	1.16	0.13	1.00	1.44	0.276
	$\delta^{18}O$ (D)	13	1.22	0.14	0.88	1.41	

Tab. 2 - Statistical comparison between ventral (V) and dorsal (D) valves of *M. venosa, A. kerguelensis, L. uva* and *L. neozelanica*. Number of results (N), mean (Mean), standard deviation (STD), minimum (Min), maximum (Max) and *p*-value for each element (Mg, Sr, Na) and stable isotopes ($\delta^{13}C$ and $\delta^{18}O$). In brown significant *p*-values, in red highly significant ones.

following major growth lines on the shell surface, without assuming that growth increments are equivalent to annual increments. Individual growth increments were separated from the shell using a scalpel, microdrill and/or razor blade and labelled 'a' for the anterior-most increment followed by 'm-1' to 'm-X', and finally by 'p' for the last increment that included the umbonal and muscle scar area (Fig. 2, Appendix 1). The number of m-1 to m-X increments sampled depended, in part, on the length as well as the thickness of the shell. In general, in the analysed specimens, the three-layer shells were thicker than their two-layer counterparts. To be noted, in the three-layer shells (*L. neozelanica* and *G. vitreus*) the powder for the analysis was collected from both the secondary and tertiary layers, thus, each sample represents both layers in varying proportions. However, the tertiary layer tends to be the dominant mass (Ye et al. 2018) and thus the prominent factor in their overall geochemistry. Posterior, middle and anterior parts were discriminated based on the curvature of the shell: umbonal curvature in the posterior region, lowest curvature in the middle part and again increase in curvature in the anterior part (Fig. 2), and ultimately on the chemical trace element and/or stable isotope trends. Each shell increment was powdered in an agate mortar and about 3-20 mg of each sample was weighed to four decimal places, and digested in 2 % (v/v) distilled nitric acid (HNO_3) with the addition of matrix modifier solutions (sample, calibration and standards) to facilitate analysis for Ca, Mg, Sr and Na by atomic absorption spectrophotometer (AAS) at Brock University, St. Catharines, Canada (cf. Brand & Veizer 1980).

Atomic Absorption Spectrometry (AAS)

All samples were analysed for Ca, Mg, Sr, and Na by AAS on a Varian 400P Spectrophotometer (Varian Medical Systems Inc., Palo Alto, USA) with appropriate gases and the addition of required matrix modifiers (cf. Brand & Veizer 1980) at the Department of Earth Sciences at Brock University, St. Catharines, Canada. Accuracy and precision of chemical analyses was determined with duplicates and standard reference material NIST NBS standard rock material 633 (Portland cement). The reproducibility (1σ) of results relative to certified values for NBS SRM 633 was 2.12 % for Ca (N=101), 1.76 % for Mg (N=108), 3.03 % for Sr (N=110) and 6.51 % for Na (N=80). Finally, all elemental results were adjusted to a 100 % carbonate basis (cf. Brand & Veizer 1980).

Mass Spectrometry

For carbon and oxygen isotope analyses about 250 µg of powdered calcite of each sample was analysed with a Finnigan GasBench connected to a Delta V (Thermo Fisher Scientific Inc., Waltham, Massachusetts, USA) mass spectrometer at the Dipartimento di Scienze della Terra, Università degli Studi di Milano, Italy. Isotope values ($\delta^{18}O$, $\delta^{13}C$) are reported as per mil (‰) deviations of the isotopic ratios ($^{18}O/^{16}O$, $^{13}C/^{12}C$) calculated to the V-PDB scale using a within-run internal laboratory standard (MAMI) calibrated against the International Atomic Energy Agency 603 standard (IAEA-603; $\delta^{18}O$: -2.37 ± 0.04 ‰, $\delta^{13}C$: +2.46 ± 0.01 ‰). Analytical reproducibility (1σ) for these analyses was better than 0.15 ‰ for $\delta^{18}O$ and 0.09 ‰ for $\delta^{13}C$ values.

Statistical analysis

The mean, standard deviation and minimum and maximum values of each element (Mg, Sr and Na) and stable isotope values ($\delta^{18}O$, $\delta^{13}C$) were calculated for each valve of each specimen and for the entire specimen (i.e., ventral and dorsal valves together; Tables 2, 3). Also, an independent-sample t-test was conducted to check if there was a significant difference in the geochemical and isotopic results, 1) between ventral and dorsal valves of the same specimen (applies to *M. venosa, L. uva, A. kerguelensis* and *L. neozelanica*) and 2) among the posterior, middle and anterior parts of the shell of the same species (Table 3). The analysis was performed using SPSS Statistics (IBM Version 22.0. Armonk,

NY). For the independent-sample t-test a *p*-value ≤ 0.05 was considered significant and a *p*-value ≤ 0.001 was considered highly significant.

RESULTS

Trace elements

•Trace elements in *M. venosa* (Fig. 3) show a slightly positive trend from the posterior to the anterior areas in both valves. When comparing the concentrations of Mg and Sr between the two valves a *p*-value of 0.564 for Mg and 0.742 for Sr indicate no significant differences between them (Table 2). In contrast, a highly significant difference is noted between the anterior and middle areas of the shell for Mg (Table 3), and also a significant difference is
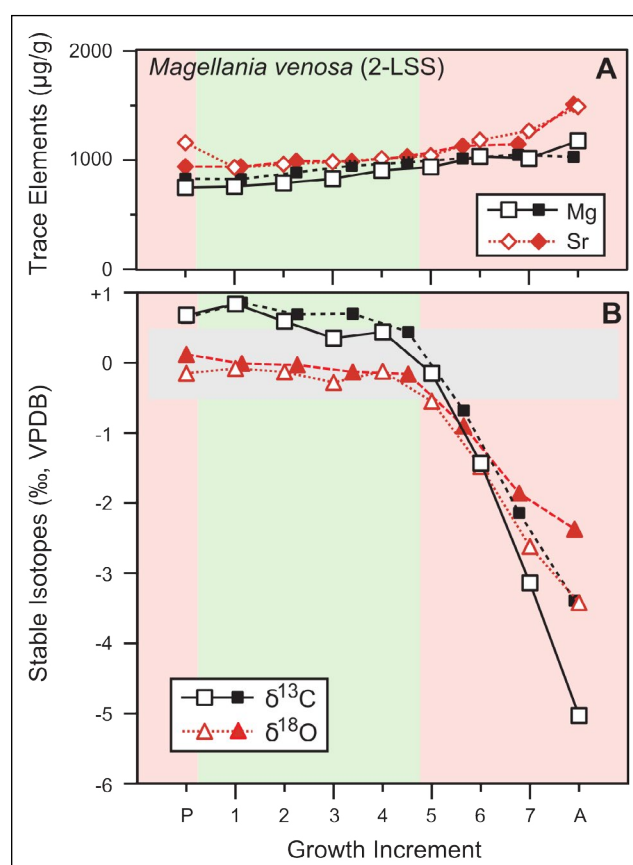

Fig. 3 - Geochemical profiles of *Magellania venosa* and its 2-layer shell sequence (2-LSS) from posterior (p) to anterior (a). A) Trace element concentration (Mg and Sr), B) Oxygen and Carbon stable isotopes. Empty symbols: ventral valve, solid symbols: dorsal valve. Pink coloured areas represent posterior and anterior regions; green area represents the mid-section of the valve. The grey horizontal box shows the brachiopod isotope equilibrium field for measured $\delta^{18}O$ values with respect to the ambient seawater-^{18}O and temperature (cf. Brand et al. 2013; Appendix 1).

Species	Parameter	N	Mean	STD	Min	Max	p
Magellania venosa	Mg (p)	2	789	56	750	829	A vs M 0.001
	Mg (m)	8	865	77	759	979	P vs M 0.238
	Mg (a)	7	1036	71	937	1176	A vs P 0.003
	Sr (p)	2	1049	154	940	1159	A vs M 0.007
	Sr (m)	8	980	34	933	1032	P vs M 0.639
	Sr (a)	7	1253	182	1041	1511	A vs P 0.199
	$\delta^{13}C$ (p)	2	0.76	0.03	0.74	0.78	A vs M 0.004
	$\delta^{13}C$ (m)	8	0.71	0.19	0.45	0.96	P vs M 0.734
	$\delta^{13}C$ (a)	7	-2.18	1.70	-4.93	-0.05	A vs P 0.053
	$\delta^{18}O$ (p)	2	0.26	0.19	0.12	0.40	A vs M 0.003
	$\delta^{18}O$ (m)	8	0.15	0.08	-0.01	0.26	P vs M 0.234
	$\delta^{18}O$ (a)	7	-1.62	1.00	-3.16	-0.28	A vs P 0.041
Liothyrella uva	Mg (p)	2	2357	29	2336	2377	A vs M 0.049
	Mg (m)	18	2345	531	1784	3155	P vs M 0.929
	Mg (a)	4	3025	833	2180	4125	A vs P 0.345
	Sr (p)	2	1166	156	1056	1276	A vs M 0.026
	Sr (m)	18	1218	133	1075	1498	P vs M 0.615
	Sr (a)	4	1411	202	1210	1652	A vs P 0.215
	Na (p)	2	2784	164	2668	2900	A vs M 0.011
	Na (m)	18	2680	297	1770	3074	P vs M 0.638
	Na (a)	4	3123	225	2827	3368	A vs P 0.138
	$\delta^{13}C$ (p)	2	1.01	0.05	0.98	1.05	A vs M 0.439
	$\delta^{13}C$ (m)	18	1.05	0.15	0.76	1.27	P vs M 0.747
	$\delta^{13}C$ (a)	4	0.80	0.55	0.32	1.31	A vs P 0.502
	$\delta^{18}O$ (p)	2	3.59	0.02	3.58	3.60	A vs M 0.697
	$\delta^{18}O$ (m)	18	3.45	0.09	3.29	3.63	P vs M 0.053
	$\delta^{18}O$ (a)	4	3.43	0.17	3.23	3.65	A vs P 0.295
Aerothyris kerguelensis	Mg (p)	2	787	13	777	796	A vs M <0.001
	Mg (m)	14	1006	199	694	1313	P vs M 0.001
	Mg (a)	4	1466	122	1321	1619	A vs P 0.002
	Sr (p)	2	800	21	786	815	A vs M <0.001
	Sr (m)	14	879	69	789	982	P vs M 0.017
	Sr (a)	4	1049	40	1003	1093	A vs P 0.001
	Na (p)	2	1366	7	1361	1371	A vs M 0.004
	Na (m)	14	1742	430	1220	2493	P vs M 0.006
	Na (a)	4	2495	179	2273	2651	A vs P 0.001
	$\delta^{13}C$ (p)	2	2.22	0.13	2.14	2.31	A vs M <0.001
	$\delta^{13}C$ (m)	14	2.63	0.10	2.42	2.78	P vs M <0.001
	$\delta^{13}C$ (a)	4	2.26	0.19	2.00	2.44	A vs P 0.812
	$\delta^{18}O$ (p)	2	2.74	0.20	2.60	2.88	A vs M 0.097
	$\delta^{18}O$ (m)	14	2.93	0.17	2.70	3.22	P vs M 0.173
	$\delta^{18}O$ (a)	4	2.76	0.15	2.65	2.97	A vs P 0.888
Liothyrella neozelanica	Mg (p)	11	1357	226	1035	1817	A vs M 0.022
	Mg (m)	14	1308	163	1109	1549	P vs M 0.531
	Mg (a)	5	2105	503	1529	2644	A vs P 0.026
	Sr (p)	11	710	54	618	789	A vs M 0.083
	Sr (m)	14	624	31	575	689	P vs M <0.001
	Sr (a)	5	790	162	571	972	A vs P 0.338
	Na (p)	10	1165	237	857	1552	A vs M 0.016
	Na (m)	13	913	88	777	1035	P vs M 0.009
	Na (a)	5	1501	333	1087	1921	A vs P 0.041
	$\delta^{13}C$ (p)	11	1.81	0.35	1.40	2.49	A vs M 0.046
	$\delta^{13}C$ (m)	14	2.70	0.12	2.50	2.89	P vs M <0.001
	$\delta^{13}C$ (a)	5	2.18	0.41	1.74	2.66	A vs P 0.083
	$\delta^{18}O$ (p)	11	1.13	0.12	0.88	1.28	A vs M 0.092
	$\delta^{18}O$ (m)	14	1.25	0.12	1.04	1.44	P vs M 0.017
	$\delta^{18}O$ (a)	5	1.14	0.12	1.00	1.31	A vs P 0.817
Gryphus vitreus	Mg (Vp)	1	2252				
	Mg (Vm)	10	653	140	553	968	M vs A 0.016
	Mg (Va)	5	2325	936	1447	3846	
	Sr (Vp)	1	825				
	Sr (Vm)	10	514	74	421	641	M vs A <0.001
	Sr (Va)	5	958	164	737	1194	
	Na (Vp)	1	1351				
	Na (Vm)	10	587	113	461	865	M vs A 0.006
	Na (Va)	5	1552	423	1120	2248	
	$\delta13C$ (Vp)	1	1.85				
	$\delta13C$ (Vm)	10	2.97	0.28	2.56	3.30	M vs A 0.029
	$\delta13C$ (Va)	5	2.56	0.36	2.04	3.00	
	$\delta18O$ (Vp)	1	2.06				
	$\delta18O$ (Vm)	10	2.14	0.21	1.83	2.43	M vs A 0.524
	$\delta18O$ (Va)	5	2.09	0.09	2.00	2.23	

Tab. 3 - Statistical comparison of trace element and stable isotope chemistry between the posterior (p), middle (m) and anterior (a) shell parts of the articulated brachiopod specimens *M. venosa, A. kerguelensis, L. uva, L. neozelanica* and *G. vitreus*. Number of samples (N), mean (Mean), standard deviation (STD), minimum (Min), maximum (Max) and *p*-values. In brown significant *p*-values, in red highly significant ones.
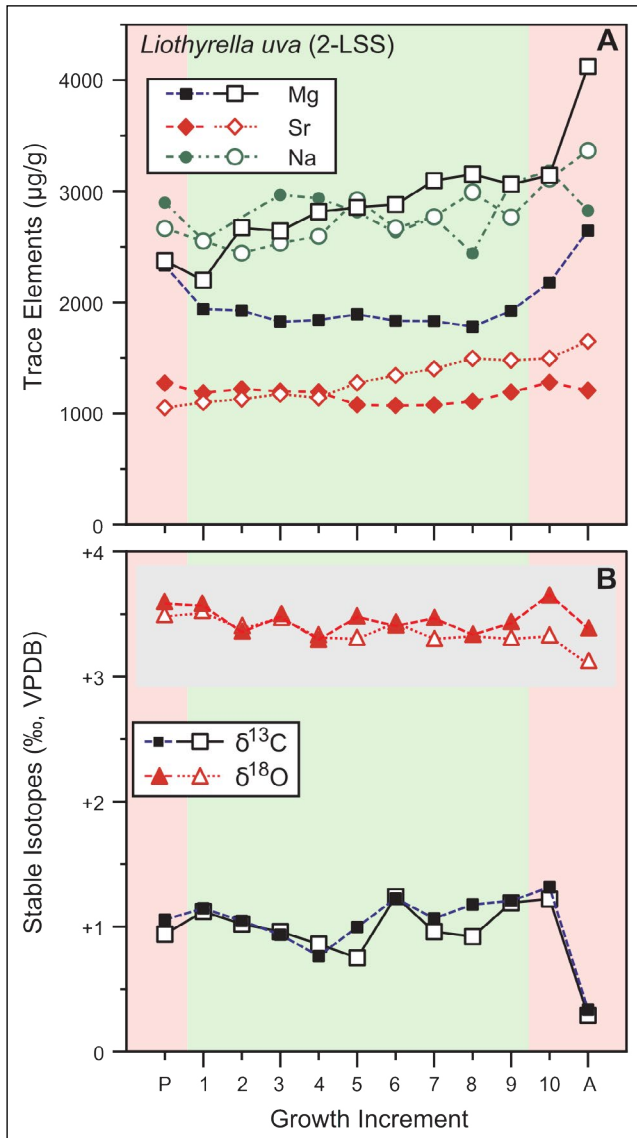
Fig. 4 - Geochemical profiles of *Liothyrella uva* and its 2-layer shell sequence (2-LSS) from posterior (p) to anterior (a). A) Trace element concentration (Mg, Sr and Na), B) Oxygen and Carbon stable isotopes. Empty symbols: ventral valve, solid symbols: dorsal valve. Pink coloured areas represent posterior and anterior regions; green area represents the mid-section of the valve. The grey horizontal box as in Figure 3.

Fig. 5 - Geochemical profiles of *Aerothyris kerguelensis* and its 2-layer shell sequence (2-LSS)) from posterior (p) to anterior (a). A) Trace element concentration (Mg, Sr and Na), B) Oxygen and Carbon stable isotopes. Empty symbols: ventral valve, solid symbols: dorsal valve. Pink coloured areas represent posterior and anterior regions; green area represents the mid-section of the valve. The grey horizontal box as in Figure 3.

found between the anterior and posterior areas for Mg, and anterior and middle areas for Sr (Table 3).

•Trace elements in *L. uva* (Fig. 4) show a slightly positive trend from the posterior to the anterior area of the shell, which is particularly evident in the divergent Mg concentrations that reach high values anteriorly of 4125 µg/g in the ventral valve and 2649 µg/g in the dorsal valve (Appendix 1). A highly significant difference for Mg concentration (p-value < 0.001) is found between ventral and dorsal valves, whereas a significant difference is observed in Sr concentrations (Table 2). When
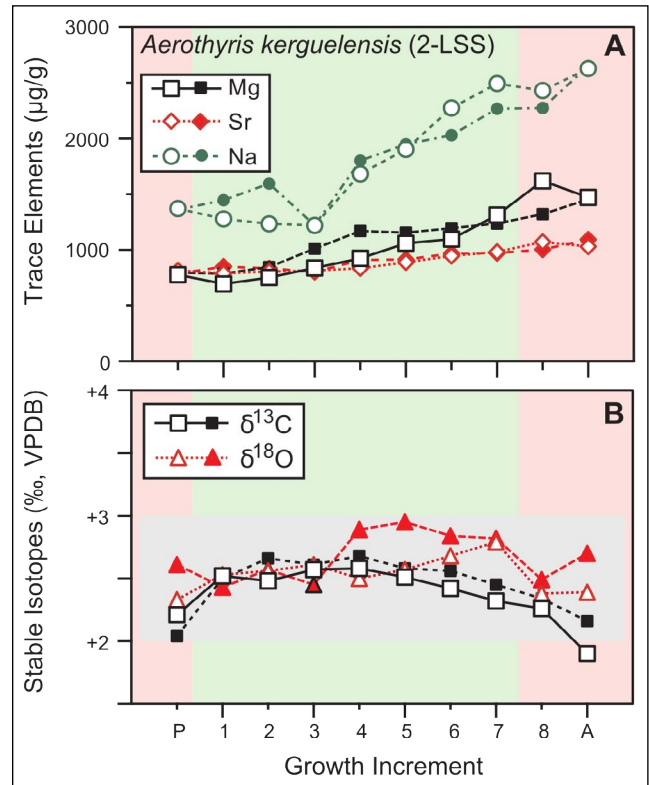
comparing the different areas of the shell, a significant difference is found between the anterior and middle area for all three elements (Table 3).

•Trace elements recorded in *A. kerguelensis* show continually slightly upward trends from the posterior region to the anterior margin in both valves (Fig. 5). The minimum and maximum concentrations are relatively comparable between the two valves (Table 2, Appendix 1); only in Mg we observe a big difference, where the ventral valve maximum value is 1619 µg/g, whereas the dorsal one is 1454 µg/g. Correlation between the two valves, relative to the investigated elements is noteworthy with p-values for the three elements as follows: 0.986 for Mg, 0.873 for Sr and 0.594 for Na, indicating no significant difference between the valves (Table 2). In contrast, the comparison between the different areas of the valve shows highly significant differences between anterior and middle areas for Mg and Sr, between posterior and middle areas for Mg, and between anterior and posterior areas for Sr
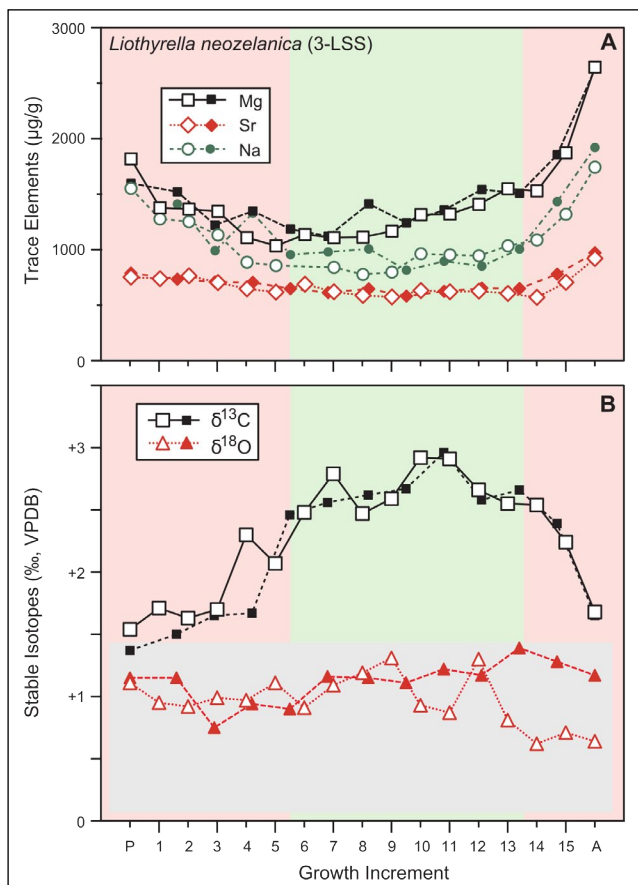
Fig. 6 - Geochemical profiles of *Liothyrella neozelanica* and its 3-layer shell sequence (2-LSS) from posterior (p) to anterior (a). A) Trace element concentration (Mg, Sr and Na), B) Oxygen and Carbon stable isotopes. Empty symbols: ventral valve, solid symbols: dorsal valve. Pink coloured areas represent posterior and anterior regions; green area represents the mid-section of the valve. The grey horizontal box as in Figure 3.

and Na. A significant difference is found between anterior and posterior areas for Mg, posterior and middle areas for Sr and Na, and anterior and middle area for Na (Table 3).

•In *L. neozelanica*, trace element trends are similar for both valves (Fig. 6), showing a U-shaped trend with higher concentration in the posterior (umbo area) and anterior area, reaching maximum values anteriorly of 2644 µg/g for Mg, 921 µg/g for Na and 1743 µg/g for Sr in the ventral valve, and of 2627 µg/g for Mg, 972 µg/g for Na and 1921 µg/g for Sr in the dorsal valve (Fig. 6, Table 2; Appendix 1). As indicated by the *p*-values no significant difference is found between ventral and dorsal valve trace-element contents (Table 2). Instead, a highly significant difference is observed between middle and posterior areas in Sr, whereas significant differences is found between anterior and middle areas in

Mg and Na, middle and posterior areas in Na, and anterior and posterior areas in Mg and Na (Table 3).

•Trace elements recorded in *G. vitreus* show a pronounced U-shaped trend, with high values in the posterior (umbo area), which then decrease in concentration reaching lowest values in the middle part of the shell with 523 µg/g for Mg, 421 µg/g for Sr and 461 µg/g for Na, and subsequently increase approaching the anterior margin, with Mg reaching 3846 µg/g, Sr up to 1194 µg/g and Na reaching 2248 µg/g (Fig. 7, Table 2; Appendix 1). A highly significant difference is present between anterior and middle areas for Sr, whereas a significant difference is found between anterior and middle areas for Mg and Na (Table 3).

Stable isotopes

•The $\delta^{18}O$ and $\delta^{13}C$ values of *M. venosa* (Fig. 3) are rather constant up to the middle part of both valves, then a sharp drop in the $\delta^{18}O$ and $\delta^{13}C$ values of both valves is observed, reaching very negative values (ventral valve: $\delta^{18}O$ = -3.16 ‰, $\delta^{13}C$ = -4.93 ‰; dorsal valve: $\delta^{18}O$ =-2.10 ‰, $\delta^{13}C$ = -3.29 ‰; Appendix 1). No significant difference is observed between ventral and dorsal valves in stable isotope values (Table 2). Instead, a significant difference is found between anterior and middle areas in their collective $\delta^{13}C$ values (p = 0.004), and anterior and middle areas (p = 0.003) and anterior and posterior areas (p = 0.041) in their $\delta^{18}O$ values (Table 3).

•Oxygen and carbon isotope compositions of *L. uva* (Fig. 4) show a rather constant trend from the umbo to the anterior part of the shell (ventral valve: maximum $\delta^{18}O$ = +3.65 ‰, minimum $\delta^{18}O$ = +3.29 ‰, maximum $\delta^{13}C$ = +1.31 ‰, minimum $\delta^{13}C$ = +0.33 ‰. Dorsal valve: maximum $\delta^{18}O$ = +3.63 ‰, minimum $\delta^{18}O$ = +3.23 ‰, maximum $\delta^{13}C$ = +1.25 ‰, minimum $\delta^{13}C$ = +0.32 ‰; Appendix 1). No significant differences are found between dorsal and ventral valves ($\delta^{18}O$, p = 0.538; $\delta^{13}C$, p = 0.832) and among the different parts of the shell (Tables 2, 3). Carbon isotope values in the anterior area record a decrease of nearly 1 ‰ both in the ventral and dorsal valves.

•The oxygen and carbon isotope values recorded in the *A. kerguelensis* specimen show similar trends in both ventral and dorsal valves (Fig. 5; Appendix 1). Oxygen values show no particular trend and remain rather constant from the umbo to the anterior part of the shell (ventral valve: maximum:

+3.06 ‰; minimum: +2.56 ‰; dorsal valve: maximum: +3.22 ‰; minimum: +2.70 ‰). Carbon values show, instead, a slightly reverse U-shaped trend with lower values in the umbo (+2.31 ‰ in the ventral valve and +2.14 ‰ in the dorsal one) and in the anterior margin (+2.00 ‰ in the ventral valve and +2.26 ‰ in the dorsal one) and higher values in the middle area of the shell (up to +2.68 ‰ in the ventral valve and +2.78 ‰ in the dorsal one). The higher *p*-values obtained ($\delta^{18}O$, $p = 0.076$; $\delta^{13}C$, $p = 0.421$) indicate that there is no significant difference between the stable isotope values of the ventral and dorsal valves (Table 2). A highly significant difference ($p < 0.001$) is found between anterior and middle areas, and posterior and middle areas in $\delta^{13}C$ values (Table 3).

•Oxygen isotope compositions in *L. neozelanica* (Fig. 6; Appendix 1) show a nearly constant trend punctuated by apparently seasonal variation, recorded by both ventral and dorsal valves (ventral valve: maximum $\delta^{18}O = +1.44$ ‰, minimum $\delta^{18}O = +1.00$ ‰; dorsal valve: maximum $\delta^{18}O = +1.41$ ‰, minimum $\delta^{18}O = +0.88$ ‰). Carbon isotopes show a distinctly reverse U-shaped trend with lower values in the umbo (+1.57 ‰ in the ventral valve and +1.40 ‰ in the dorsal one) and in the anterior area (+1.76 ‰ in the ventral valve and +1.74 ‰ in the dorsal one) reaching higher values in the middle area of the shell, up to +2.82 ‰ in the ventral valve and +2.89 ‰ in the dorsal valve. No significant difference is found between the dorsal and ventral valves ($\delta^{18}O$, $p = 0.276$; $\delta^{13}C$, $p = 0.729$) (Table 2). Instead, a significant difference is observed between the posterior and middle areas ($p = 0.017$) in $\delta^{18}O$ values and anterior and middle areas ($p = 0.046$) in $\delta^{13}C$ values, whereas a highly significant difference is found between the posterior and middle area ($p < 0.001$; Table 3).

•Oxygen isotope compositions in *G. vitreus* (Fig. 7; Appendix 1) do not record a peculiar trend, remaining nearly constant from the umbo to the anterior part of the shell (maximum $\delta^{18}O = +2.43$ ‰, minimum $\delta^{18}O = +1.83$ ‰). In contrast, carbon isotope values, instead, show a reverse U-shaped trend, similar to the one observed in *L. neozelanica*, with lower values in the umbo (+1.85 ‰) and in the anterior area (+2.04 ‰) and higher values in the middle of the shell (up to +3.30 ‰) (Fig. 7; Appendix 1). A significant difference is found between anterior and middle areas in $\delta^{13}C$ values (Table 3).
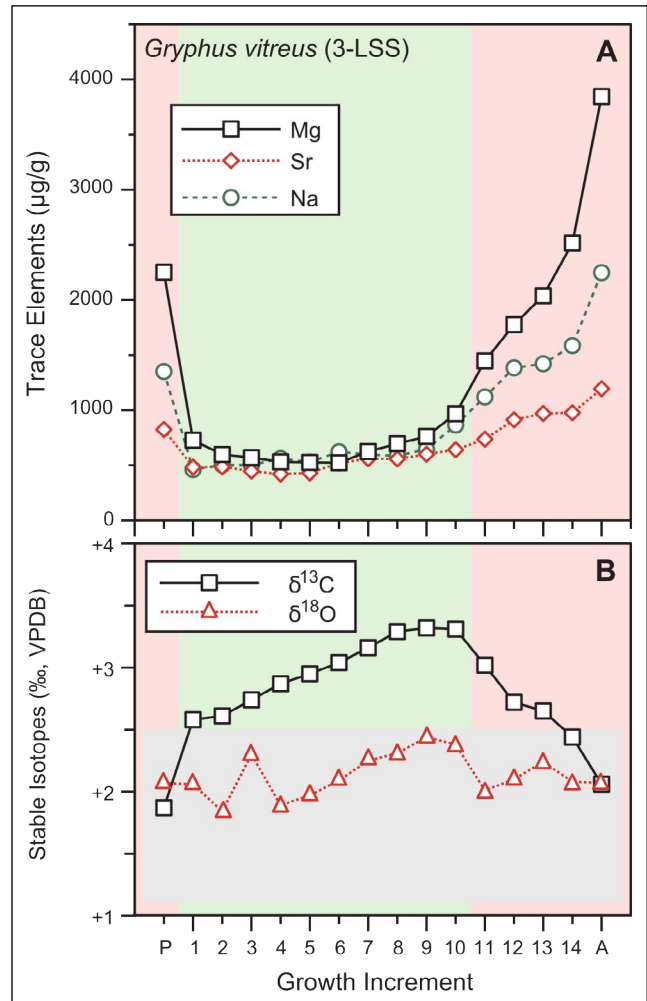

Fig. 7 - Geochemical profiles of *Gryphus vitreus* and its 3-layer shell sequence (2-LSS) from posterior (p) to anterior (a). A) Trace element concentration (Mg, Sr and Na), B) Oxygen and Carbon stable isotopes. Empty symbols: ventral valve, solid symbols: dorsal valve. Pink coloured areas represent posterior and anterior regions; green area represents the mid-section of the valve. The grey horizontal box as in Figure 3.

DISCUSSION

Two-layer vs. three-layer shells

Comparable trends have been observed in the trace element concentrations and stable isotope values recorded along the growth axis by the two-layer *vs.* three-layer shells. For this reason, the following discussion will be organized along the groups *G. vitreus* and *L. neozelanica*, with a columnar tertiary layer (Gaspard 1991), and *A. kerguelensis, M. venosa* and *L. uva*, with only primary and secondary layers (Williams & Cusack 2007).

As shown in Figures 6 and 7, trace element concentrations for both three-layer shells of *L. neozelanica* and *G. vitreus* show a U-shaped trend, which

is particularly evident for Mg. Higher concentrations are recorded in the posterior region, they then decrease toward the middle of the shell and increase again toward the anterior margin, where they reach their highest concentrations. In *G. vitreus* this trend is highly emphasized, with Mg and Sr concentrations respectively increasing more than 7 and 2.5 times between their lowest and their maximum values. A reverse U-shaped trend is recorded in the δ^{13}C values in both species, similar to that observed in other studies by Takayanagi et al. (2013) and Takizawa et al. (2017). The observed trends may be explained considering the three-layer structure of *L. neozelanica* and *G. vitreus* and the current sampling strategy, which collected shell powders from both the secondary and tertiary layers. The tertiary layer is generally depleted in trace elements (Milner et al. 2017) and has a lower organic content compared to the secondary layer, where the organic matter is present as organic sheaths around the fibres (intercrystalline matrix) and within the punctae in punctate brachiopods, such as terebratulid brachiopods (Gaspard et al. 2007; Pérez-Huerta et al. 2009). Only impersistent organic sheets between the tertiary columns have been observed (Williams et al. 1997; Schmahl et al. 2012). According to Garbelli et al. (2014), the greater amount of organic matter may be related to vital processes and this may be reflected in the carbon isotope compositions of the shell calcite. In fact, metabolic respiration and photosynthesis may cause shifts in the δ^{13}C values of the shells without having an apparent impact on their δ^{18}O compositions (McConnaughey 1989). The normal and reverse U-shaped trends observed in trace elements and carbon isotope values are thus related to the different distribution of the tertiary and secondary layers in the shells. The maximum thickness of the tertiary layer is in the middle part of the shell, where *L. neozelanica* and *G. vitreus* recorded comparatively lower trace element contents and higher δ^{13}C values, whereas in the anterior area, where the secondary layer is dominant, higher concentrations of trace elements and lower δ^{13}C values are observed. Similarly low δ^{13}C values and high trace elements concentrations (mainly Mg) are recorded also in the posterior umbonal area. This part represents a specialized area of the shell, where cardinal structure and muscle scars are present. As described by other studies (e.g., Parkinson et al. 2005; Takizawa et al. 2017) specialized areas have generally low δ^{13}C val-

ues in agreement with the present observations. Although carbon isotopes and elemental contents exhibit clear trends, δ^{18}O values for both *G. vitreus* and *L. neozelanica* remain relatively stable and seem not to correlate with the other trace element and δ^{13}C trends (Figs. 6 and 7). Their variations appear not to be related to microstructural changes and shell successions, and thus, δ^{18}O potentially records environmental changes that occurred during the life of the organism (cf. Veizer & Prokoph 2015).

The two-layer shells of *L. uva* and *A. kerguelensis* (Figs. 4, 5) do not show any U-shaped trends (normal or reverse) in their trace element and stable isotope records, as has been observed in the three-layer shells. This may be also due to the relatively uniform ambient water conditions (temperature), and low metabolism and slow growth rates (cf. *L. uva* at Rothera, Peck et al. 1997).

Trace elements in both species show a general increasing trend from the umbo to the anterior margin, which is especially evident in the Mg content. However, Mg concentrations of *L. uva* are much higher compared to the ones of *A. kerguelensis*. Cusack et al. (2008) have observed in *Terebratalia trasversa* that Mg may be associated with organic components, and since *L. uva* has a greater organic content than other recent species (Ye et al. 2018), this may explain our results. Stable isotope values remain rather constant through the shell of both species, with carbon being slightly more variable than oxygen, but in both cases having a less than 1 ‰ variation along the shell. In the δ^{13}C values of *A. kerguelensis* a similar reverse U-shaped trend to those observed in *G. vitreus* and *L. neozelanica* is recorded, although much less pronounced. The sampling of specialized areas in the posterior part and a decrease due to metabolic effect in the anterior area may account for these low values (cf. Parkinson et al. 2005; Takayanagi et al. 2013; Takizawa et al. 2017). The significant drop in δ^{13}C values of 0.98 ‰ (ventral valve) and 0.93 ‰ (dorsal valve) in the anterior area of *L. uva* may be the result of primary layer contamination during sampling - a distinct possibility due the extreme thinness of the shell - or may be due to a metabolic effect. The decrease in ^{13}C incorporation into shells at a mature age has been reported in brachiopods (Yamamoto et al. 2010, 2013; Takayanagi et al. 2012, 2013; Takizawa et al. 2017) and bivalves (Lorrain et al. 2004; Freitas et al. 2005). As the organism grows and become older, its metabolism increases while shell growth slows;

so the amount of available metabolic CO_2 increases, while the amount needed for shell growth is reduced, resulting in more metabolic carbon (^{12}C enriched), being incorporated into the shell (Lorrain et al. 2004). Generally, in the two-layer shells, trace elements and $\delta^{13}C$ values show a more stable pattern throughout the shell. With regards to trace element contents, different authors described different trends through the shells especially focusing on Mg. Some authors (e.g., Takizawa et al. 2017; Ullmann et al. 2017) observed an increase in their concentrations at the anterior margin, whereas others noticed the opposite (e.g., Buening & Carlson 1992). As reported by Cusack & Williams (2007) and Cusack et al. (2008), the Mg distribution within the shell is not even and may have unpredictable variations, and its concentration may not only be linked to shell growth rate but may be incorporated in different ways in different ontogenetic parts of the shell. Milner et al. (2017) showed that trace elements varied in the different shell layers and explained this variation as possibly due to modifications in the chemical composition of the biological fluids during biomineralization.

A separate discussion is required for the two-layer shell of *M. venosa* (Fig. 3, Suppl. Fig. 1). Trace elements display a pattern similar to that observed in the other brachiopod species of this study, of a slightly increasing trend from the umbo to the anterior margin. In contrast, oxygen and carbon isotope values show a peculiar behaviour. Their values remain quite stable up to the middle of the shell, then they suddenly drop by up to 5 ‰ in both valves and both isotopes (Fig. 3). A similarly perplexing trend is also observed in the carbon and oxygen isotopes of a mature specimen of *M. venosa* with many plateaus and negative isotope excursions, although less pronounced in terms of ‰ variations (Suppl. Fig. 1).

A first explanation for this sudden shift towards lighter isotopic values may be contamination with the primary layer material. This is a possibility, although, we strictly followed the cleaning protocol of Zaky et al. (2015). Incorporation of some minute amounts of powder from the primary layer – possibly entrapped inside the growth lamellae (Fig. 8) - may not cause the significant variations in both $\delta^{18}O$ and $\delta^{13}C$ values because of the large difference in mass between the two layers. Similar negative isotope excursions were also recorded by Ullmann et al. (2017; their Fig. 6) in their mature specimen of *M. venosa* from the South American shelf. The spec-
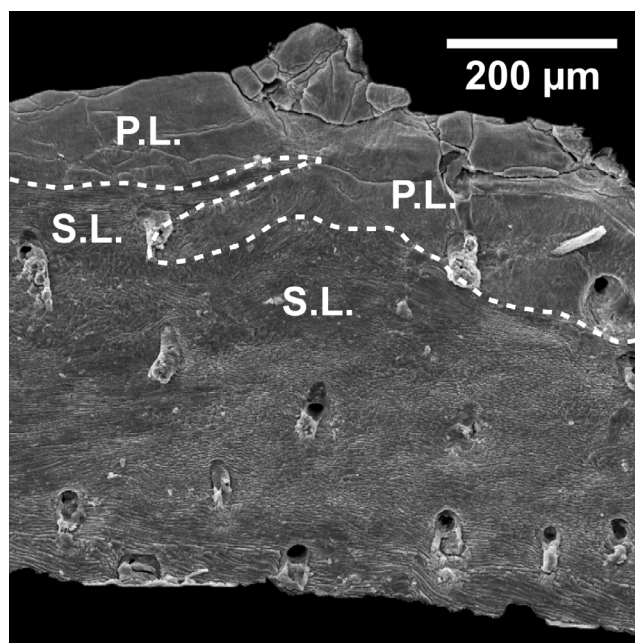

Fig. 8 - Scanning electron microscope (SEM) image of microstructural layers in *L. uva*. Image shows the primary layer calcite intruding into the fibres of the secondary layer corresponding to the position of a growth lamella. This results in an uneven boundary transition between the primary and outermost secondary layers in brachiopods, and possibly corresponds to isotope irregularities (cf. Yamamoto et al. 2010). PL: primary layer, SL: secondary layer.

imen analysed in this study is a juvenile specimen (Fig. 3, 37 mm, Table 1), while the other (~70 mm, Table 1; Suppl. Fig. 1) and the one of Ullmann et al. (2017) are mature ones. Comparing our stable isotope trends with the ones of Ullmann et al. (2017), we noted the same significant drop in isotope values in the first part of the shell (juvenile part) and latter part of the mature one, also in terms of ‰ variation (up to 4 ‰ for $\delta^{18}O$ and up to 6 ‰ for $\delta^{13}C$ in Ullmann et al. 2017). However, Ullmann et al. (2017) did not discuss in detail the observed trend, pointing only to possible shell secretion in disequilibrium with ambient seawater. It may be hypothesised that this behaviour is species-specific, or it may be related to specific environmental perturbations which characterise the environment of *M. venosa*. According to Försterra et al. (2008), large accumulations of *M. venosa* were found in Comau and Reñihué fjords (42° to 43° South, southern Chile), areas characterised by a high productivity especially in summer and deep-water upwelling. Shifts in nearshore productivity and higher temperatures linked to the El Niño-Southern Oscillation (ENSO), occurring on interannual and decadal timescales, have
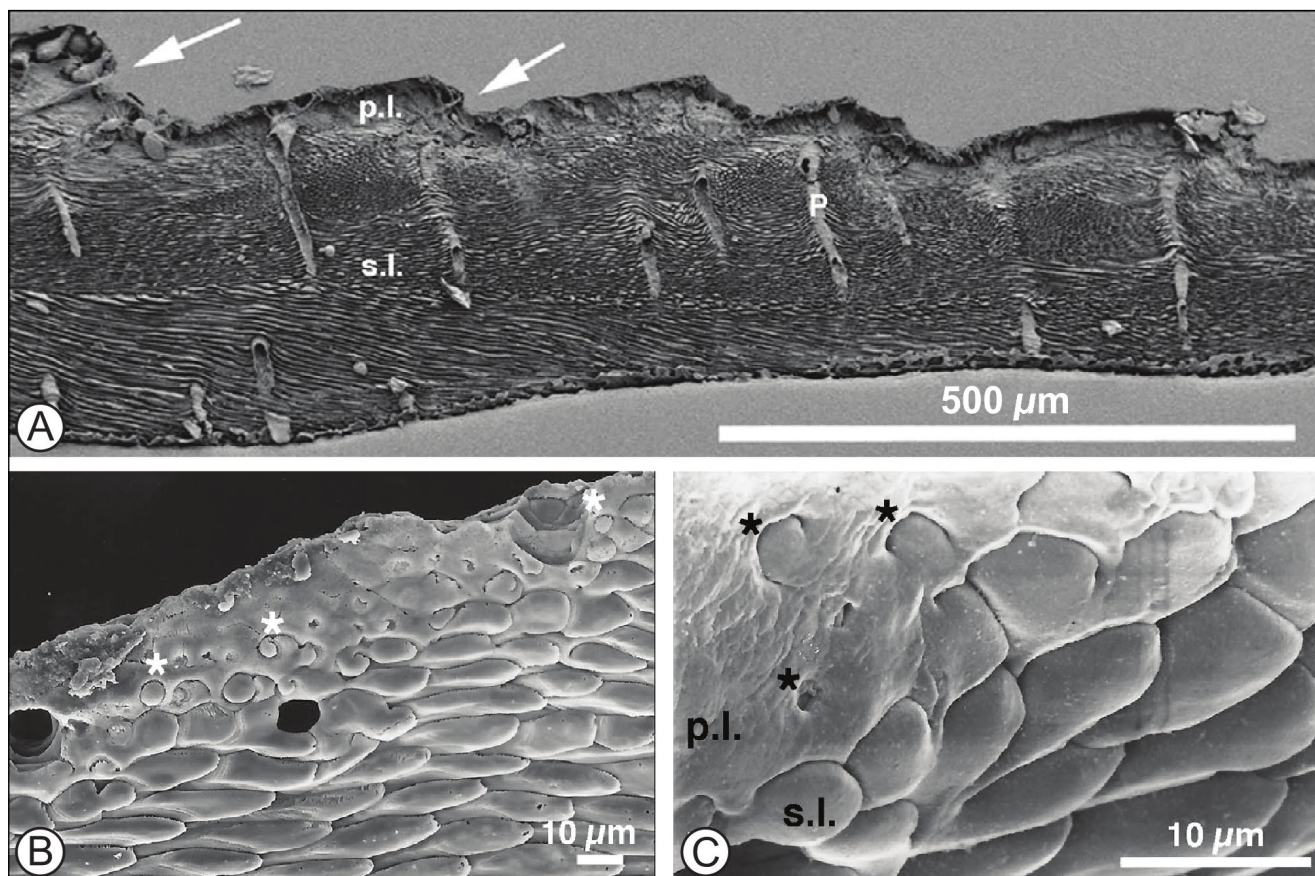
Fig. 9 - Scanning electron microscope (SEM) images of shell cross-sections showing microstructures in *A. kerguelensis, G. vitreus* and *L. neozelanica* (arrows, modified after Gaspard & Nouet 2016). A) growth lamellae with primary layer calcite into fibres of the secondary layer in *A. kerguelensis*, B) transitional contact between the primary and secondary layers in *G. vitreus* (white stars), C) transitional contact between the primary and secondary layers in *L. neozelanica* (black stars). The tertiary layer is not represented in the images. Note: p.l. - primary layer, s.l. - secondary layer, p - punctae.

been observed along the Chilean coast (e.g. Ulloa et al. 2001; Takesue et al. 2004), possibly affecting the geochemical signatures recorded by the brachiopod shells. Furthermore, effects on benthic organisms of the Patagonian fjord region were observed during the intense development of anthropogenic activities (aquaculture, shellfish harvesting) over the past two decades (Buschmann et al. 2006; Mayr et al. 2014; Försterra et al. 2014, 2016). In 2003, three small salmon farms were operating in Comau Fjord, whereas in 2017, 23 very large farms were actively using their concessions (Häussermann, pers. observation). For example, a significant depletion of mussels, gorgonians, large deepwater sea anemones, calcifying ectoprocts, and decapods was observed, probably caused by eutrophication and increased sedimentation and/or the increase of event-based adding of chemical substances during the salmonid farming process (Häussermann et al. 2013). Coral mass mortality along a 14 km stretch of Comau

fjord shoreline was documented for 2012 (Försterra et al. 2014), probably after an intense algae bloom. Mayr et al. (2014) showed that primary production in Comau fjord has doubled during the last two decades. The developments in Comau Fjord also may have caused a deviation of the geochemical signatures with respect to shell parts precipitated under undisturbed conditions. However, for the evaluation of the different possibilities and to better understand the causes of the drop, more specimens of *M. venosa* need to be analysed.

Which is the best or optimal part of the shell for geochemical analysis?

Independent-sample t-tests performed on trace elements and stable isotopes recorded by the specimens, highlight that there is no significant difference between dorsal and ventral valves, with the exception of the Mg concentration in *L. uva* (Tables 2, 3). This is in agreement with previous stud-

ies which found no difference in the geochemistry (Parkinson et al. 2005; Brand et al. 2015) and in the morphometry of the fibres of the secondary layer (Ye et al. 2018) between ventral and dorsal valves. This means that for terebratulids, which possess valves with similar shell layer succession and general shape, both ventral and dorsal valves can be used for geochemical analyses. However, this may not be the case for the other brachiopod taxa in the fossil record. Representatives of Palaeozoic orders such as the Productida have valves strongly different in terms of shape and microstructure (i.e., species of the genus *Gigantoproductus;* Angiolini et al. 2012; Nolan et al. 2017) and thus record a different primary geochemical signature. Also, they may undergo different degrees of diagenetic alteration which in turn control their ultimate geochemical record (Garbelli et al. 2014).

Here, we proved that, not only the posterior (umbonal) area and primary layer of the shell have to be avoided as previously mentioned by several authors (e.g., Carpenter & Lohmann 1995; Brand et al. 2003; Parkinson et al. 2005; Griesshaber et al. 2007; Pérez-Huerta et al. 2008), but care has to be taken also when using the anterior part of the shell for geochemical analyses. In fact, significant geochemical differences have been found between the different areas of the shells in nearly all geochemical signatures (trace elements and carbon isotopes) of the five studied brachiopod species. $\delta^{18}O$ values seem to remain generally stable throughout the overall shell, whereas both two- and three-layer shell successions exhibit greater stability in their trace element and carbon isotope records in the middle of the shells. This is in agreement with observations by Butler et al. (2015), who documented a certain stability in the $\delta^{18}O$ values recorded along the growth axis in their specimens of *L. neozelanica* and *Terebratulina retusa*. These results are also supported by the study of Takizawa et al. (2017), which showed that the intrashell and intraspecific $\delta^{18}O$ and $\delta^{13}C$ variations of the middle part of the shell were small compared to those in the anterior and posterior sections. This suggests that this portion provides reliable results for palaeoenvironmental investigations. Besides removal of the out of disequilibrium primary layer, the outermost part of the secondary layer should be chemically etched to avoid possible contamination by the intrusion of the primary layer in correspondence of growth lamellae (Figs 8, 9). Also, the

external part of the secondary layer may have been secreted in disequilibrium with the ambient seawater (e.g., Auclair et al. 2003; Parkinson et al. 2005; Cusack et al. 2012; Takizawa et al. 2017). According to Cusack et al. (2012) only the innermost fibres of the secondary layer of mature specimens should be included in proxy calculations of seawater temperature. The calcitic fibres produced early in ontogeny are likely to be isotopically light, thus resulting in higher/warmer calculated seawater temperatures.

Furthermore, in fossil brachiopods, the outermost and innermost part (outer rims) of the whole shell may be more prone to diagenetic alteration as testified by Figure 10. Carboniferous brachiopods from England (Stephenson et al. 2010), analysed by cathodoluminescence, show a highly luminescent innermost shell rim (Fig. 10). In fact, the outermost and innermost parts of shells, as well as the posterior and particularly the thinner anterior regions, may be more directly affected by diagenetic fluids, and thus be the first to be altered.

Therefore, it is recommended to focus sampling for geochemical analysis, both in recent and fossil specimens, to the middle part of the shell of both valves, avoiding the posterior and anterior regions as well as the outermost and innermost parts, and potentially other areas (cf. Casella et al. 2018).

Summary and Conclusions

In this study, we analysed the trace element contents (Mg, Sr, Na) and stable isotope compositions ($\delta^{18}O$, $\delta^{13}C$) of five recent brachiopod species (*M. venosa, L. uva, A. kerguelensis, L. neozelanica* and *G. vitreus*) collected from different latitudes and different environments (Chile, Antarctica, Indian Ocean, New Zealand and Italy). Three-layer shells of *L. neozelanica* and *G. vitreus* show characteristic trends (i.e., normal and reverse U-shaped trend) in their geochemical signatures compared to that of the two-layer shells of *L. uva* and *A. kerguelensis*, mainly due to the different incorporation of trace elements and different carbon isotope fractionation, in the secondary and tertiary layers. Among the two-layer shells, *M. venosa* shows a sudden change in stable isotopes at mid-shell length in both juvenile and mature specimens. Further studies are necessary to confirm our findings and adequately evaluate the causes for the observed geochemical profiles.
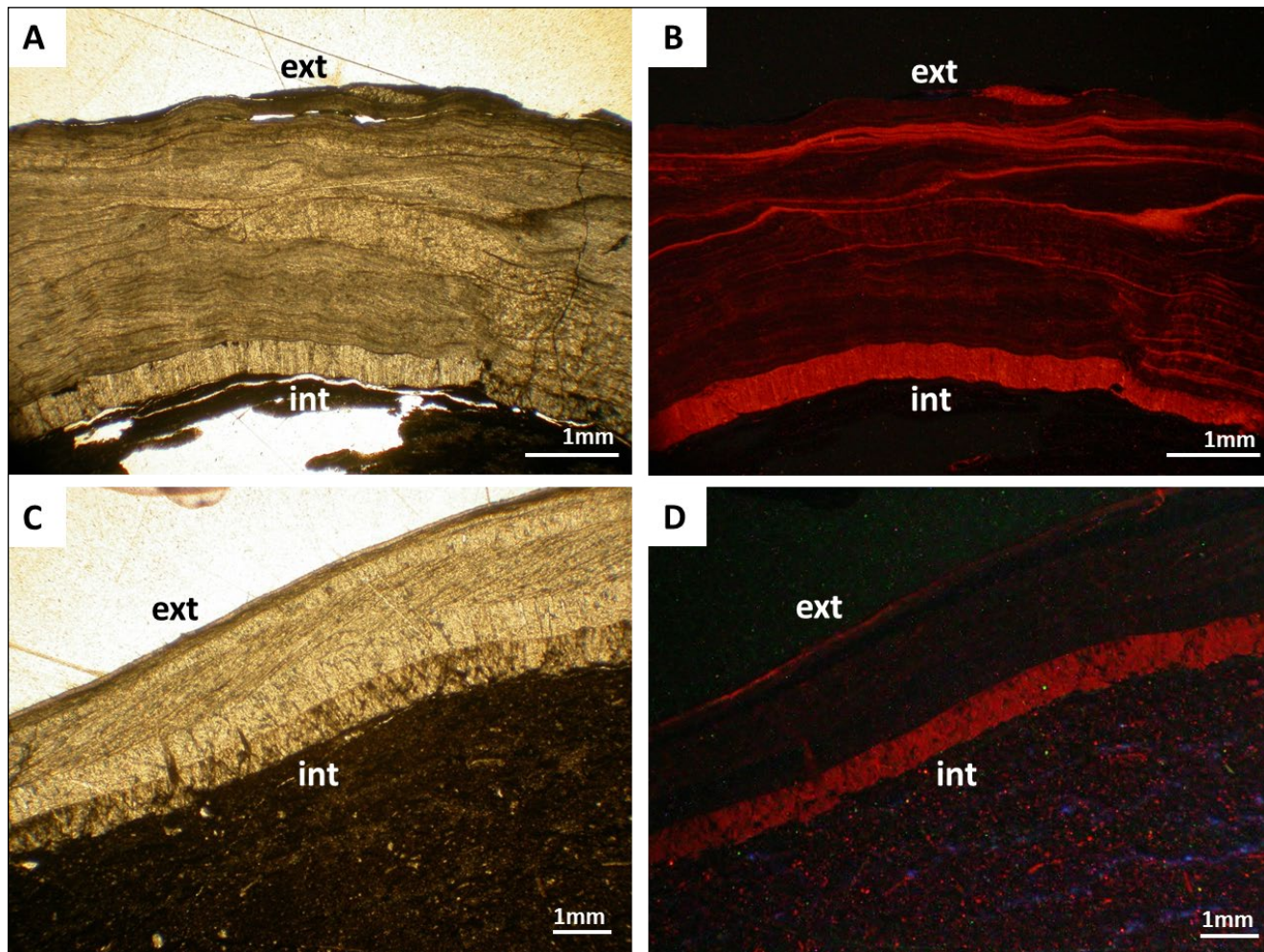
Fig. 10 - Primary and diagenetic features in fossil brachiopods. Transmitted light (A, C) and cathodoluminescence (B, D) photomicrographs. Note that in both specimens the innermost and outermost rims of the shell luminesce due to recrystallization and incorporation of manganese in the calcite of the shell (Brand & Veizer 1980). The outer shell may reflect the readily altered primary layer, whereas the innermost part reflects a zone of the secondary/tertiary layer more prone to diagenetic alteration; a layer in direct contact with diagenetic fluids circulating through the sediment column (cf. Casella et al. 2018). A, B: *Antiquatonia hindi;* C, D: *Skelidorygma* sp., Yoredale cyclothems, Serpukhovian, Carboniferous, NE England (Stephenson et al. 2010). Ext: external part of valve; int: internal part of valve.

The results of the analyses undertaken on shells of both groups led us to observe that data obtained from geochemical and isotope analyses performed on the posterior and anterior areas of shells should be interpreted with care, as the incorporation of trace elements and stable isotopes in these regions may be controlled and affected by the organism metabolism. Also for fossil specimens, the outermost and innermost parts of the shells, as well as the posterior and anterior region, should be avoided as they may be the first parts to be diagenetically altered, yielding erroneous results. Of note is the trend observed in $\delta^{18}O$ values in nearly all the species, which remain quite stable throughout the shells, being less affected by the microstructure or the organism's metabolism and being thus a most reliable tool for (palaeo)climatic reconstructions. So

in pristine fossil brachiopods oxygen isotopes can be considered good proxies of palaeoenvironmental and palaeoclimatic conditions. Diagenesis can obscure the original signal, but it can be easily screened (e.g. Angiolini et al. 2009; Brand et al. 2011; Crippa et al. 2016b). Although diagenesis may reset primary values, it may preserve their cyclicity or trend of variation (Angiolini et al. 2012).

In addition to proper cleaning and sample preparation procedures, for both recent and fossil brachiopod specimens, it is also very important to define 1) the microstructure and shell succession, and 2) the best part of the shell where to safely perform geochemical and isotope analyses. The middle region of the shell, which represents the most stable part from a geochemical and isotopic point of view, should be used for analyses.

REFERENCES

Angiolini L., Darbyshire D.P.F., Stephenson M.H., Leng M.J., Brewer T.S., Berra F. & Jadoul F. (2008) - Lower Permian brachiopods from Oman: their potential as climatic proxies. *Earth. Env. Sci. T. R. So.*, 98: 327-344.

Angiolini L., Jadoul F., Leng M.J., Stephenson M.H., Rushton J., Chenery S. & Crippa G. (2009) - How cold were the Early Permian glacial tropics? Testing sea-surface temperature using the oxygen isotope composition of rigorously screened brachiopod shells. *J. Geol. Soc.*, 166 (5): 933-945.

Angiolini L., Stephenson M., Leng M.J., Jadoul F., Millward D., Aldridge A., Andrews J., Chenery S. & Williams G. (2012) - Heterogeneity, cyclicity and diagenesis in a Mississippian brachiopod shell of palaeoequatorial Britain. *Terra Nova*, 24: 16-26.

Auclair A.C., Joachimski M.M. & Lécuyer C. (2003) - Deciphering kinetic, metabolic and environmental controls on stable isotopic fractionations between seawater and the shell of *Terebratalia transversa* (Brachiopoda). *Chem. Geol.*, 202: 59-78.

Azmy K., Brand U., Sylvester P., Gleson S.A., Logan A. & Bitner M.A. (2011) - Biogenic and abiogenic low-Mg calcite (bLMC and aLMC): evaluation of seawater-REE composition, water masses and carbonate diagenesis. *Chem. Geol.*, 280: 180-190.

Bajnai D., Fiebig J., Tomasovych A., Milner Garcia S., Rollion-Bard C., Raddatz J., Löffler N., Primo-Ramos C. & Brand U. (2018) - Assessing kinetic fractionation in brachiopod calcite using clumped isotopes. *Scientific Reports*, 8: 1-12.

Brand U. (2004) - Carbon, oxygen and strontium isotopes in Paleozoic carbonate components: an evaluation of original seawater-chemistry proxies. *Chem. Geol.*, 204: 23-44.

Brand U. & Veizer J. (1980) - Chemical diagenesis of a multicomponent carbonate system: 1, trace elements. *J. Sediment. Petrol.*, 50: 1219-1236.

Brand U. & Veizer J. (1981) - Chemical diagenesis of a multicomponent carbonate system: 2, stable isotopes. *J. Sediment. Petrol.*, 51: 987-997.

Brand U., Logan A., Hiller N. & Richardson J. (2003) - Geochemistry of modern brachiopods: applications and implications for oceanography and paleoceanography. *Chem. Geol.*, 198: 305-334.

Brand U., Logan A., Bitner M.A., Griesshaber E., Azmy K. & Buhl D. (2011) - What is the ideal proxy of Palaeozoic seawater chemistry? *Assoc. Australas. Paleontol. Mem.*, 41: 9-24.

Brand U., Azmy K., Bitner M.A., Logan A., Zuschin M., Came R. & Ruggiero E. (2013) - Oxygen isotopes and $MgCO_3$ in brachiopod calcite and a new paleotemperature equation. *Chem. Geol.*, 359: 23-31.

Brand U., Azmy K., Griesshaber E., Bitner M.A., Logan A., Zuschin M., Ruggiero E. & Colin P.L. (2015) - Carbon isotope composition in modern brachiopod calcite: a case of equilibrium with seawater? *Chem. Geol.*, 411: 81-96.

Buening N. & Carlson S.J. (1992) - Geochemical investigation of growth in selected recent articulate brachiopods. *Lethaia*, 25: 331-345.

Buschmann A.H., Riquelme V.A., Hernández-González M.C., Varela D., Jiménez J.E., Henríquez L.A., Vergara P.A., Guíñez R. & Filún L. (2006) - A review of the impacts of salmon farming on marine coastal ecosystems in the southeast Pacific. *ICES J. Marine Sci.*, 63: 1338-1345.

Butler S., Bailey T., Lear C.H., Curry G.B., Cherns L. & McDonald I. (2015) - The Mg/Ca temperature relationship in brachiopod shells: calibrating a potential palaeoseasonality proxy. *Chem. Geol.*, 397: 106-117.

Came R.E., Eiler J.M., Veizer J., Azmy K., Brand U. & Weidman C.R. (2007) - Coupling of surface temperatures and atmospheric CO_2 concentrations during the Palaeozoic era. *Nature*, 449: 198-202.

Carpenter S.J. & Lohmann K.C. (1995) - $\delta^{18}O$ and $\delta^{13}C$ values of modern brachiopod shells. *Geochim. Cosmochim. Acta*, 59 (18): 3749-3764.

Casella L., Griesshaber E., Simonet Roda M., Ziegler A., Mavromatis V., Henkel D., Laudien J., Häussermann V., Neuser R.D., Angiolini L., Dietzel M., Eisenhauer A., Immenhauser A., Brand U. & Schmahl W.W. (2018) - Micro- and nanostructures reflect the degree of diagenetic alteration in modern and fossil brachiopod shell calcite: a multi-analytical screening approach (CL, FE-SEM, AFM, EBSD). *Palaeogeogr., Palaeoclimatol., Palaeoecol.*, in press.

Crippa G., Ye F., Malinverno C. & Rizzi A. (2016a) - Which is the best method to prepare invertebrate shells for SEM analysis? Testing different techniques on recent and fossil brachiopods. *Boll. Soc. Paleontol. Ital.*, 55: 111-125.

Crippa G., Angiolini L., Bottini C., Erba E., Felletti F., Frigerio C., Hennissen J.A.I., Leng M.J., Petrizzo M.R., Raffi I., Raineri G. & Stephenson M.H. (2016b) - Seasonality fluctuations recorded in fossil bivalves during the early Pleistocene: Implications for climate change. *Palaeogeogr., Palaeoclimatol., Palaeoecol.*, 446, 234-251.

Curry G.B. & Brunton C.H.C. (2007) - Stratigraphic distribution of brachiopods. In: Selden P.A. (Ed.) - Treatise

on Invertebrate Paleontology. Part H. Brachiopoda Revised: 2901-2965. Geol. Soc. Am. & Univ. Kansas, New York.

Cusack M. & Williams A. (2007) - Biochemistry & diversity of brachiopod shells. In: Selden P.A. (Ed.) - Treatise on Invertebrate Paleontology Part H, Brachiopoda Revised: 2373-2395. Geol. Soc. Am. & Univ. Kansas, New York.

Cusack M., Pérez-Huerta A., Janousch M. & Finch A.A. (2008) - Magnesium in the lattice of calcite-shelled brachiopods. *Chem. Geol.,* 257: 59-64.

Cusack M. & Pérez-Huerta A. (2012) - Brachiopods recording seawater temperature – a matter of class or maturation? *Chem. Geol.,* 334: 139-143.

Emig C.C., Bitner M.A. & Álvarez F. (2013) - Phylum Brachiopoda. In: Zhang Z-Q. (Ed.) - Animal Biodiversity: An Outline of Higher-level Classification and Survey of Taxonomic Richness. *Zootaxa,* 3703: 75-78.

Försterra G., Häussermann V. & Lueter C. (2008) - Mass occurrence of the recent brachiopod *Magellania venosa* (Terebratellidae) in the fjords Comau and Renihue, northern Patagonia, Chile. *Mar Ecol.,* 29: 342-347.

Försterra G., Häussermann V., Laudien J., Jantzen C., Sellanes J. & Muñoz P. (2014) - Mass die-off of the cold-water coral *Desmophyllum dianthus* in the Chilean Patagonian fjord region. *Bull. Mar. Sci.,* 90: 895-899.

Försterra G., Häussermann V. & Laudien J. (2016) - Animal Forests in the Chilean fjords: discoveries, perspectives and threats in shallow and deep waters. In: Rossi S., Bramanti L., Gori A. & Orejas Saco del Valle C. (Eds) - Marine Animal Forests – The Ecology of Benthic Biodiversity Hotspots. Springer International Publishing, Switzerland.

Freitas P., Clarke L. J., Kennedy H., Richardson C. & Abrantes F. (2005) - Mg/Ca, Sr/Ca, and stable-isotope (δ^{18}O and δ^{13}C) ratio profiles from the fan mussel *Pinna nobilis*: seasonal records and temperature relationships. *Geochem. Geophys. Geosyst.,* 6: Q04D14.

Garbelli C., Angiolini L., Brand U. & Jadoul F. (2014) - Brachiopod fabric, classes and biogeochemistry: implications for the reconstruction and interpretation of seawater carbon-isotope curves and records. *Chem. Geol.,* 371: 60-67.

Garbelli C., Angiolini L. & Shen S.Z. (2017) - Biomineralization and global change: a new perspective for understanding the end-Permian extinction. *Geology,* 45: 19-12.

Gaspard D. (1986) - Aspects figurés de la biominéralisation – Unités de base de la secretion carbonatée chez des Terebratulida actuels. In: Racheboeuf P.R., Emig C. (Eds) - Les Brachiopodes fossiles et actuels. Actes du 1er Congrès International sur les Brachiopodes, Brest. *Biostratig. Paléozoïque*: 77-83.

Gaspard D. (1991) - Growth stages in articulate brachiopod shells and their relation to biomineralization. In: MacKinnon, D.I., Lee, D.E. & Campbell, J.D. (Eds) - Brachiopod through time: 167-174. Balkema, Rotterdam.

Gaspard D. & Nouet J. (2016) - Hierarchical architecture of the inner layers of selected extant rhynchonelliform brachiopods. *J. Struct. Biol.,* 196: 197-205.

Gaspard D., Marie B., Guichard N., Luquet G. & Marin F. (2007) - Biochemical characteristics of the shell soluble organic matrix of some recent rhynchonelliformea (Brachiopoda). Biomineralization: from Paleontology to materials science. In: Proceedings of the 9th International Symposium on Biomineralization: 193-204.

Griesshaber E., Schmahl W.W., Neuser R., Pettke T., Blum M., Mutterlose J. & Brand U. (2007) - Crystallographic texture and microstructure of terebratulide brachiopod shell calcite: an optimized materials design with hierarchical architecture. *Am. Mineral.,* 92: 722-734.

Grossman E.L., Zhang C. & Yancey T.E. (1991) - Stable-isotope stratigraphy of brachiopods from Pennsylvanian shales in Texas *Geol. Soc. Amer. Bull.,* 103: 953-965.

Häussermann V., Försterra G., Melzer R.R. & Meyer R. (2013) - Gradual changes of benthic biodiversity in Comau fjord, Chilean Patagonia – lateral observations over a decade of taxonomic research. *Spixiana,* 36(2): 161-71.

Locarnini R.A., Mishonov A.V., Antonov J.I., Boyer T.P., Garcia H.E., Baranova O.K., Zweng M.M., Paver C.R., Reagan J.R., Johnson D.R., Hamilton M. & Seidov D. (2013) - World Ocean Atlas 2013, Volume 1: Temperature. NOAA Atlas NESDIS 73: 40.

Lorrain A., Paulet Y.M., Chauvaud L., Dunbar R., Mucciarone D. & Fontugne M. (2004) - δ^{13}C variation in scallop shells: increasing metabolic carbon contribution with body size? *Geochim. Cosmochim. Acta,* 68: 3509-3519.

Lowenstam H.A. (1961) - Mineralogy, O^{18}/O^{16} ratios, and strontium and magnesium contents of recent and fossil brachiopods and their bearing on the history of the oceans. *J. Geol.,* 69: 241-260.

Mayr C.C., Rebolledo L., Schulte K., Schuster A., Zolitschka B., Fösterra G. & Häusserman V. (2014) - Responses of nitrogen and carbon deposition rates in Comau Fjord (42°S, Southern Chile) to natural and anthropogenic impacts during the last century. *Cont. Shelf Res.,* 78: 29-38.

McConnaughey T. (1989) - ^{13}C and ^{18}O isotopic disequilibrium in biological carbonates: I. Patterns. *Geochim. Cosmochim. Acta,* 53: 151-162.

Milner S., Rollion-Bard C., Burckel P., Tomašových A., Angiolini L. & Henkel D. (2017) - Assessing the biomineralization processes in the shell microstructure of modern brachiopods: variations in the oxygen isotope composition and minor element ratios. *EGU General Assembly Conference Abstracts*, 19: 6455.

Parkinson D., Curry G.B., Cusack M. & Fallick, A.E. (2005) - Shell structure, patterns and trends of oxygen and carbon stable isotopes in modern brachiopod shells. *Chem. Geol.,* 219: 193-235.

Peck L.S., Brockington S. & Brey T. (1997) - Growth and metabolism in the Antarctic brachiopod *Liothyrella uva. Phil. Trans. Royal Soc. London*, B352: 851-858.

Pérez-Huerta A., Cusack M., Jeffries T. & Williams T. (2008) - High resolution distribution of magnesium and strontium and the evaluation of Mg/Ca thermometry in Recent brachiopod shells. *Chem. Geol.,* 247: 229-241.

Pérez-Huerta A., Cusack M., McDonald S., Marone F., Stampanoni M. & MacKay S. (2009) - Brachiopod punctae: a

complexity in shell biomineralisation. *J. Struct. Biol.,* 167: 62-67.

Popp B.N., Anderson T.F. & Sandberg P.A. (1986) - Brachiopods as indicators of original isotopic compositions in some Paleozoic limestones. *Geol. Soc. Am. Bull.*, 97: 1262-1269.

Rollion-Bard C., Saulnier S., Vigier N., Schumacher A., Chaussidon M. & Lécuyer C. (2016) - Variability in magnesium, carbon and oxygen isotope compositions of brachiopod shells: implications for paleoceanographic studies. *Chem. Geol.,* 423: 49-60.

Schmahl W.W., Griesshaber E., Kelm K., Goetz A., Jordan G., Ball A., Xu D., Merkel C. & Brand U. (2012) - Hierarchical structure of marine shell biomaterials: biomechanical functionalization of calcite by brachiopods. *Z. Kristallog. Cryst. Mater.*, 227: 793-804

Stephenson M.H., Angiolini L., Cózar P., Jadoul F., Leng M. J., Millward D. & Chenery S. (2010) - Northern England Serpukhovian (early Namurian) farfield responses to southern hemisphere glaciation. *J. Geol. Soc.,* 167: 1171-1184.

Takayanagi H., Asami R., Abe O., Kitagawa H., Miyajima T. & Iryu Y. (2012) - Carbon- and oxygen-isotope compositions of a deep-water modern brachiopod *Campagea japonica* collected off Aguni-jima, Central Ryukyu Islands, southwestern Japan. *Geochem. J.,* 46: 77-87.

Takayanagi H., Asami R., Abe O., Miyajima T., Kitagawa H., Sasaki K. & Iryu Y. (2013) - Intraspecific variations in carbon isotope and oxygen-isotope compositions of a brachiopod *Basiliola lucida* collected off Okinawa-jima, southwestern Japan. *Geochim. Cosmochim. Acta.*, 115: 115-136.

Takesue R., Van Geen A., Carriquiry J., Ortiz E., Godinez-Orta L., Granados I., Saldívar M., Ortlieb L., Escribano R., Guzmán N., Castilla J., Varas M., Salamanca M. & Figueroa C. (2004) - Influence of coastal upwelling and El Niño-Southern Oscillation on nearshore water along Baja California and Chile: shore-based monitoring during 1997-2000. *J. Geophys. Res.,* 109: 1-14.

Takizawa M., Takayanagi H., Yamamoto K., Abe O., Sasaki K. & Iryu Y. (2017) - Paleoceanographic conditions at approximately 20 and 70ka recorded in *Kikaithyris hanzawai* (Brachiopoda) shells. *Geochim. Cosmochim. Acta*, 215: 189-213.

Ullmann C.V., Frei R., Korte C. & Lüter, C. (2017) - Element/Ca, C and O isotope ratios in modern brachiopods: species-specific signals of biomineralisation. *Chem. Geol.,* 460: 15-24.

Ulloa O., Escribano R., Hormazabal S., Quinones R.A., González R.R. & Ramos M. (2001) - Evolution and biological effects of the 1997-98 El Niño in the upwelling ecosystem off northern Chile. *Geophys. Res. Lett.,* 28: 1591-1594.

Veizer J. (1992) - Depositional and diagenetic history of limestones: stable and radiogenic isotopes. In: Clauer N. & Chaudhuri S. (Eds) - Isotopic Signatures and Sedimentary Records: 13-48. Springer-Verlag, Berlin.

Veizer J. & Prokoph A. (2015) - Temperatures and oxygen isotopic composition of Phanerozoic oceans. *Earth-Sci. Rev.,* 146: 92-104.

Veizer J., Ala D., Azmy K., Bruckschen P., Buhl D., Bruhn F., Carden G.A.F., Diener A., Ebneth S., Godderis Y., Jasper T., Korte C., Pawellek F., Podlaha O.G. & Strauss H. (1999) - $^{87}Sr/^{86}Sr$, $\delta^{13}C$ and $\delta^{18}O$ evolution of Phanerozoic seawater. *Chem. Geol.,* 161: 59-88.

Williams A. & Cusack M. (2007) - Chemicostructural diversity of the brachiopod shell. In: Selden P.A. (Ed.) - Treatise on Invertebrate Paleontology. Part H. Brachiopoda Revised: 497-502. Vol. 6. Geol. Soc. Am. & Univ. Kansas, Boulder, Colorado & Lawrence, Kansas.

Williams A., Brunton C.H.C., Carlson S.J. and 44 authors (1997) - Introduction (part). In: Kaesler R.L. (Ed.) - Treatise on Invertebrate Paleontology, Part H, Brachiopoda revised. Geol. Soc. Am. & Univ. Kansas, New York.

Yamamoto K., Asami R. & Iryu Y. (2010) - Within-shell variations in carbon and oxygen isotope compositions of two modern brachiopods from a subtropical shelf environment off Amami-oshima, southwestern Japan. *Geochem., Geophys., Geosys.*, 11(10): 1-16.

Yamamoto K., Asami R. & Iryu Y. (2013) - Correlative relationships between carbon-and oxygen-isotope records in two cool-temperate brachiopod species off Otsuchi Bay, northeastern Japan. *Paleontol. Res.,* 17: 12-26.

Ye F., Crippa G., Angiolini L., Brand U., Capitani G., Cusack M., Garbelli C., Griesshaber E., Harper E. & Schmahl W. (2018) - Mapping of recent brachiopod microstructure: A tool for environmental studies. *J. Struct. Biol.,* 201: 221-236.

Zaky A.H., Brand U. & Azmy K. (2015) - A new sample processing protocol for procuring seawater REE signatures in biogenic and abiogenic carbonates. *Chem. Geol.*, 416: 36-50.